Knotted spacetime electromagnetic vortex unlinking and unknotting with vector and scalar reconnections and field twist compensation

Jordan M. Adams *
Riverside Research, Beavercreek, Ohio 45431, USA

(Received 24 April 2026; accepted 25 September 2026; published 9 November 2026)

Optical vortex knots have been realized in monochromatic laser beams, but monochromatic fields are stationary and their topology is frozen. Here we show that knotted spatiotemporal vortices, whose phase singularities form closed loops in space-time, undergo topology-changing reconnections with free-space propagation. When null lines of different vector components unlink, the electric spin, magnetic spin, linear momentum, and electromagnetic helicity densities, each built from a specific pair of field components, twist to exactly compensate the change in linking number. This compensation is enforced by the argument principle, where the total for each component pair, combining mutual phase twist, geometric linking, and open-line threading, vanishes identically and remains exactly zero through all reconnection events.

DOI: 10.1103/ny6g-sm2k

I. INTRODUCTION

In classical fluids, the helicity $\mathcal{H} = \int \mathbf{v} \cdot \boldsymbol{\omega} d^3x$, where $\mathbf{v}$ is the velocity and $\omega = \nabla \times \mathbf{v}$ is the vorticity, is approximately conserved through reconnections [1,2], with the Călugăreanu–White–Fuller theorem decomposing helicity into the topological and geometric properties of linking, writhe, and twist [3,4]. Magnetic helicity obeys an analogous approximate conservation in plasmas [5,6]. In both systems, however, conservation degrades with viscosity or resistivity and is exact only in the dissipationless limit.

Optical vortex lines, the phase singularities of complex wave fields [7], can be knotted and linked in monochromatic beams [8–10] and carry topological textures such as polarization skyrmions [11,12]. A vortex line is locally characterized by its topological charge and local anisotropy ellipse; phase twist describes rotation of a constant-phase ribbon along the line, whereas twirl describes rotation of the anisotropy ellipse [13,14]. The present work focuses on phase twist.

Monochromatic fields, however, are stationary, and their vortex topology cannot change. Berry & Dennis proved that the phase twist of a closed dislocation loop equals the dislocation strength threading through the loop [7], applying Cauchy's argument principle to wave singularities, and Dennis connected this to the Călugăreanu relation, $L_s = \Theta + W$, for phase ribbons, where L_s is the self-linking number, Θ is the phase twist, and W is the writhe. This relation shows that writhe must compensate changes in phase twist and vice versa [13]. These results establish identities for a single scalar field at a fixed instant but do not address conservation through topology-changing reconnection.

Spatiotemporal optical vortices, polychromatic beams whose phase singularities exist as lines in (x, y, t) at each propagation plane z, have finite extent and can undergo reconnection as z changes [15,16]. Recent measurements have also resolved ultrafast phase-singularity annihilation dynamics [17]. Spatiotemporal vortex knots were first constructed numerically from Milnor polynomials and were shown to unknot through reconnection upon propagation [18]. Additionally, spatiotemporally localized optical links and knots have been demonstrated experimentally as iso-intensity structures [19] rather than null-line vortex knots. These reconnections change the knot topology, but Maxwell's equations couple all six electromagnetic components $(E_x, E_y, E_z, B_x, B_y, B_z)$, each with its own family of null lines. Whether exact conservation laws govern this process, analogous to helicity conservation in fluids but without the approximation, has remained an open question.

Here we show that, for pairs of field components, the combination of mutual phase twist, geometric linking, and open-line threading vanishes identically and remains exactly zero through all reconnection events. The mutual phase twist between component pairs is encoded in physical observables including electric spin, magnetic spin, linear momentum, and electromagnetic helicity. When null lines of different components unlink, the Stokes vectors defining the observables acquire twist to exactly compensate the change in linking number, providing a measurable signature of exact topological conservation in electromagnetic reconnection.

Spatiotemporal fields like these knotted spatiotemporal vortices hold promise in several applications such as free-space communications, but the complicated evolution with propagation makes this an undeveloped area. We believe this work provides an initial theoretical foundation for knotted spatiotemporal vortices and their use in future

*Contact author: jadams@riversideresearch.org

Published by the American Physical Society under the terms of the Creative Commons Attribution 4.0 International license. Further distribution of this work must maintain attribution to the author(s) and the published article's title, journal citation, and DOI.

applications. Additionally, fluid reconnection processes are clouded by dissipation and nonlinearities. These results from deterministic electromagnetic propagation may give insight into fluid reconnections.

II. METHODS

Field construction and propagation. The Milnor polynomial (6, 7) is multiplied by a Gaussian envelope $g = \exp[-(r/w_0)^2 - (t/T_0)^2]$ and Fourier-transformed to the spectral domain $(\mathbf{k}, \omega)$. Propagation to distance z applies the exact transfer function $H = \exp(ik_z z)$ with $k_z = [(\omega/c)^2 - k_x^2 - k_y^2]^{1/2}$; evanescent components ($k_z^2 < 0$) are set to zero. The six field components are obtained from $\hat{E}_i = -i\omega\,(\hat{A}_i - k_i\,\mathbf{k}\cdot\hat{\mathbf{A}}/k^2)$, $\hat{\mathbf{B}} = (\mathbf{k}/\omega)\times\hat{\mathbf{E}}$. The computation uses $N_x = N_y = N_t = 384$ grid points in space and time.

Null-line detection and tracing. Null lines of each component are detected on the three-dimensional (3D) (x, y, t) grid by finding intersections of $\mathrm{Re}\,\Phi = 0$ and $\mathrm{Im}\,\Phi = 0$ contours on two-dimensional (2D) slices at multiple time values. Seed points are refined by Newton correction and connected into continuous curves by predictor-corrector marching with step size $ds = [(8\tau_X)^2 + (8\tau_y)^2 + (8c\tau_t)^2]^{1/2}$ μm, where $\tau = [\tau_x, \tau_y, \tau_t] = \frac{\nabla\mathrm{Re}\,\phi\times\nabla\mathrm{Im}\,\phi}{|\nabla\mathrm{Re}\,\phi\times\nabla\mathrm{Im}\,\phi|}$ is the normalized tangent. For polynomials with $m \geqslant 2$, closely spaced null sheets cause standard Newton correction to hop between sheets. We use a constrained corrector that projects onto the plane perpendicular to the local tangent direction: $[(\nabla\mathrm{Re}\,\Phi)^T;\ (\nabla\mathrm{Im}\,\Phi)^T;\ \hat{\tau}^T]\,\delta\mathbf{r} = [-\mathrm{Re}\,\Phi;\ -\mathrm{Im}\,\Phi;\ 0]$. Curves are validated by confirming closure (endpoint gap < 0.05) and checking that the field residual along each curve remains below 10^{-5}.

Linking numbers. The mutual linking number $L(a, b)$ is computed from the Gauss double integral $L = (4\pi)^{-1} \oint\oint(\mathbf{r}_1 - \mathbf{r}_2)\cdot(d\mathbf{r}_1 \times d\mathbf{r}_2)/|\mathbf{r}_1 - \mathbf{r}_2|^3$. The self-linking number L_s is the Gauss linking integral between the curve and a parallel-transport push-off with holonomy correction, at distance $\epsilon = 0.05$ mm.

Twist. The mutual twist $\Theta(b\,|\,a)$ is computed by evaluating the complex field Φ_b at each point of curve γ_a via trilinear interpolation on the 3D grid and summing the wrapped phase increments $\Delta\phi_i = \arg(\Phi_{b,i+1}/\Phi_{b,i})$. The total twist is $\Theta = (2\pi)^{-1}\sum_i \Delta\phi_i$. The self-phase twist is computed identically, but evaluating Φ_a along the push-off curve (at the same $\epsilon = 0.05$ mm used for L_s) rather than along γ_a itself, where the field vanishes. For a nonplanar loop, the push-off normal is first parallel transported along the curve using a rotation-minimizing frame [20]. The accumulated holonomy is then distributed continuously along the curve so that the push-off closes. For sufficiently small ε, the push-off remains disjoint from the null line and Φ_a is nonzero along it, so the phase is nonsingular. The parallel transport and offset distance ε are defined in physical (x, y, ct) coordinates.

Open-line threading. Open null lines, which do not close into loops, are detected by scanning for phase singularities (winding $> \pi$) near the pulse center in each (x, y) time slice. The threading number $\mathcal{T}_{ab}$ is computed by fan-triangulating a surface from the centroid of each closed curve and counting signed intersections of the traced open line with this surface.

III. RESULTS

In two dimensions, Cauchy's argument principle states that the phase winding of a meromorphic complex function along a closed contour counts the enclosed zeros minus the enclosed poles [21]. Although poles can arise in vortex fields [22] and ratios of vector components, this work focuses solely on zeros in the electromagnetic field components. Applied to electromagnetic vortices, this means the phase twist of a vortex loop counts the singularities that thread through the loop [7]. When the contour is a closed curve in three-dimensional space, winding counts become linking numbers [23]. If $\Phi_b(\mathbf{r})$ is a complex field whose zero set consists of N closed curves γ_b^n, $n : \{1, 2, \ldots, N\}$, then the total twist or phase winding of Φ_b along any closed curve γ_a of another field $\Phi_a(\mathbf{r})$ is

$$\Theta(b\,|\,a) \;\equiv\; \sum_n \frac{1}{2\pi}\oint_{\gamma_a^n} \mathrm{d}[\arg\Phi_b], \tag{1}$$

and the total Gauss linking number [24]

$$L(\gamma_a, \gamma_b) = \sum_n\sum_m \frac{1}{4\pi}\oint_{\gamma_a^m}\oint_{\gamma_b^n} \frac{(\mathbf{r}_1 - \mathbf{r}_2)\cdot(d\mathbf{r}_1 \times d\mathbf{r}_2)}{|\mathbf{r}_1 - \mathbf{r}_2|^3}. \tag{2}$$

Applied to the six electromagnetic components $\Phi_a \in \{E_x, E_y, E_z, B_x, B_y, B_z\}$, each with null curves γ_a^n, this yields 36 mutual twists $\Theta(b\,|\,a)$ that we collect into a 6×6 winding matrix $\Theta_{ab} = \Theta(b\,|\,a)$, where row a selects the null curves of field Φ_a and column b the sum of accumulated twist value of field Φ_b along the null lines of Φ_a. For example, $\Theta(E_x, E_y)$ measures how many multiples of 2π the phase of E_x winds around all of the closed null lines of E_y. Combining the twist matrix with the Gauss linking matrix $L_{ab} = L(\gamma_a, \gamma_b)$ defines a conservation matrix based on the argument principle

$$\mathcal{C} = \Theta + L + \mathcal{T}, \tag{3}$$

where $\mathcal{T}$ is the threading matrix. Not all null lines close into loops. Components whose null set includes open lines, singularities that extend through the domain without closing, contribute a threading number $\mathcal{T}_{ab}$ equal to the number of times these open lines pierce any surface bounded by the closed loops [24]. Equation (3) is the component-pair form of the argument principle where phase winding along the closed null loops of one component is balanced by linking with the closed null lines and signed threading by the open null lines of the other component, using a consistent orientation convention. We demonstrate numerically below that $\mathcal{C}_{ab} = 0$ for all a, b. The closed-loop contribution $\mathcal{C}^l_{ab} = \Theta_{ab} + L_{ab}$ is independently conserved under propagation, but nonzero, with $\mathcal{T}_{ab}$ providing the constant offset.

Each entry of Θ encodes a distinct physical observable, because familiar electromagnetic quantities are built from relative phases between field components, and the argument principle decomposes each relative phase into winding-matrix entries. Since $\arg(\Phi_a^*\Phi_b) = \arg\Phi_b - \arg\Phi_a$, the winding along any closed curve γ separates as

$$\frac{1}{2\pi}\oint_\gamma \mathrm{d}[\arg(\Phi_a^*\Phi_b)] = \Theta(b\,|\,\gamma) - \Theta(a\,|\,\gamma). \tag{4}$$

TABLE I. Decomposition of electromagnetic observables into winding-matrix entries via Eq. (5). Each observable has phase angle $\arg(\Phi_a^*\Phi_b)$, whose winding on γ_a is a difference of mutual and self-twists.

Observable	Phase angle	Phase winding on γ_i	Twist relation
Electric spin	$\arg(E_i^*E_j)$	$\Theta(E_j \mid E_i) - \Theta(E_i \mid E_i)$	$L_{E_i,E_i} - L_{E_i,E_j} + \mathcal{T}_{E_i,E_i} - \mathcal{T}_{E_i,E_j}$
Momentum	$\arg(E_i^*B_k)$	$\Theta(B_k \mid E_i) - \Theta(E_i \mid E_i)$	$L_{E_i,E_i} - L_{E_i,B_k} + \mathcal{T}_{E_i,E_i} - \mathcal{T}_{E_i,B_k}$
EM helicity	$\arg(E_i^*B_i)$	$\Theta(B_i \mid E_i) - \Theta(E_i \mid E_i)$	$L_{E_i,E_i} - L_{E_i,B_i} + \mathcal{T}_{E_i,E_i} - \mathcal{T}_{E_i,B_i}$
Magnetic spin	$\arg(B_i^*B_j)$	$\Theta(B_j \mid B_i) - \Theta(B_i \mid B_i)$	$L_{B_i,B_i} - L_{B_i,B_j} + \mathcal{T}_{B_i,B_i} - \mathcal{T}_{B_i,B_j}$

The twist of a bilinear observable $\arg(\Phi_a^*\Phi_b)$ at a null line is the number of 2π phase windings accumulated along the null line. Evaluating on a single null of Φ_a gives

$$\frac{1}{2\pi}\oint_{\gamma_a^n} \mathrm{d}[\arg(\Phi_a^*\Phi_b)] = \Theta(b \mid a)|_{\gamma_a^n} - \Theta(a \mid a)|_{\gamma_a^n}, \tag{5}$$

where $\Theta(a \mid a)|_{\gamma_a^n}$ is the self-twist on the null line γ_a^n. Each pair of components (a, b) defines a Poincaré sphere through the Stokes parameters $S_1 = |\Phi_a|^2 - |\Phi_b|^2$, $S_2 = 2\,\mathrm{Re}(\Phi_a^*\Phi_b)$, $S_3 = 2\,\mathrm{Im}(\Phi_a^*\Phi_b)$, with $\arg(\Phi_a^*\Phi_b) = \arctan(S_3/S_2)$ as the azimuthal coordinate. Equation (5) counts how many times this Stokes vector winds around the poles of the Poincaré sphere along a null line [25,26]. For E-E pairs, the sphere describes the polarization state, and the electric spin density is its S_3 component, $2\,\mathrm{Im}(E_i^*E_j)$ (Table I). For E-B pairs, $S_3 = 2\,\mathrm{Im}(E_i^*B_i)$ gives the helicity density and $S_2 = 2\,\mathrm{Re}(E_j^*B_k)$ gives the momentum density or Poynting vector. For B-B pairs, S_3 gives the magnetic spin. Each observable's twist is constrained by the Eq. (5) argument-principle relation. For example, the electric-spin phase-angle relation is $\frac{1}{2\pi}\oint_{\gamma_i^n} \mathrm{d}[\arg(E_i^*E_j)] = L_{E_i,E_i} - L_{E_i,E_j} + \mathcal{T}_{E_i,E_i} - \mathcal{T}_{E_i,E_j}$.

To validate the theory, we construct spatiotemporal knotted vortices based on Milnor polynomials [10,27]. We start with a scalar seed field

$$\Psi(\mathbf{r}, t) = [\alpha\, \tilde{p}^m + \tilde{q}^n] e^{-\frac{r^2}{w_0^2}} e^{-\frac{t^2}{T_0^2}} e^{-i\omega_0 t}, \tag{6}$$

with dimensionless variables

$$\tilde{p} = \frac{r^2 - r_0^2}{w_0^2} + i\frac{t}{T_0}, \quad \tilde{q} = \frac{i(x + iy)}{w_0}, \tag{7}$$

and use common lab parameters for ultrashort THz pulses: $r_0 = 1.0$ mm, $w_0 = 2.0$ mm, $T_0 = 2.0$ ps, $\alpha = 2^{2m-n}$, $\omega_0 = k_0 c$ with $k_0 = 10\ \mathrm{mm}^{-1}$. The zero set of the polynomial factor is a (m, n) torus knot or link in (x, y, t). Varying (m, n) produces the unknot, Hopf link, trefoil, and higher torus knots.

The seed Ψ is embedded in a vector potential with near-circular polarization and a small longitudinal tilt: $\hat{\mathbf{A}} = (1/\sqrt{2},\ i/\sqrt{2},\ \epsilon_{\mathrm{az}})\,\hat{\Psi}$, where $\epsilon_{\mathrm{az}} = 0.2$, and the hat symbol denotes the three-dimensional Fourier transform representation of the field in k_x, k_y, ω. The tilt breaks the degeneracy between transverse and longitudinal components, giving each an independent null-line topology. The six field components are obtained from $\hat{E}_i = -i\omega\,(\hat{A}_i - k_i\,\mathbf{k}\cdot\hat{\mathbf{A}}/k^2)$, $\hat{\mathbf{B}} = (\mathbf{k}/\omega) \times \hat{\mathbf{E}}$, and propagated using the angular spectrum method with $k_z = [(\omega/c)^2 - k_x^2 - k_y^2]^{1/2}$.

The trefoil beam $f = p^2 + q^3$ is tracked through free-space propagation (Fig. 1). At small z, the E_x null line is a trefoil knot linked three times with the E_z inner loop, while the open E_z null line threads through all closed curves [Fig. 1(a)]. With propagation, mutual reconnection reduces the cross-vector linking from 3 to 0 [Figs. 1(a)–1(c)]. The Stokes twist $\arg(E_zE_x^*)$ accumulated along each null line redistributes to compensate [Fig. 1(g)]. At each reconnection, the twist jumps by exactly one unit, as the argument principle enforces integer steps. Cross sections perpendicular to the null-line crossing [Figs. 1(j)–1(l)] show the electric spin Stokes twist $\arg(E_zE_x^*)$. At the E_x null line, E_x vanishes and this phase is undefined. Circling the null lines, the E_x-E_z Stokes vector wraps the Poincaré sphere once, giving skyrmion number [12] $N_{\mathrm{sky}} = (4\pi)^{-1}\int \mathbf{S}\cdot(\partial_u\mathbf{S}\times\partial_v\mathbf{S})du\,dv \approx 1$ (see the Supplemental Material (SM) [28]). At the reconnection, the two skyrmion lines intersect, and a skyrmion dipole annihilates and reforms afterward. At $z \approx 3$, the E_x trefoil itself reconnects, splitting into two daughter loops [Figs. 1(d)–1(f)] with a change in its own linking and corresponding redistribution of phase twist and Stokes twist [Figs. 1(h) and 1(i)], as well as skyrmion dipole annihilation [Figs. 1(m)–1(o)]. The null-line evolution is shown in SM Video 1 [28].

Tracking all six components and computing the mutual linking, mutual twist, self-phase twist, self-linking (L_s), and open-line threading (see Methods) at every propagation distance confirms the full Eq. (3) conservation matrix (Fig. 2). Additionally, the mutual linking between null lines within one vector component is plotted (L_m) and receives a double count from the double sum in Eq. (2). The E_x self-conservation $\mathcal{C}(E_x, E_x) = 0$ holds exactly through both reconnection events [Fig. 2(a)]. For E_z, which has two loops (larger outer loop not shown in Fig. 1), the closed-loop part $\mathcal{C}^l = -2$ is offset by the open-line threading $\mathcal{T}(E_z, E_z) = +2$, giving $\mathcal{C}(E_z, E_z) = 0$ [Fig. 2(b)]. The mutual conservation $\mathcal{C}(E_x, E_z) = 0$ is also verified at every z, as L drops Θ compensates exactly [Fig. 2(c)]. Defining $\mathcal{H}_l$ and $\mathcal{H}_{\mathrm{th}}$ as the total closed-loop and total threading contributions, respectively, and summing all entries of $\mathcal{C}$ gives the total

$$\mathcal{H} = \sum_{a,b} \mathcal{C}_{ab} = \mathcal{H}_l + \mathcal{H}_{\mathrm{th}} = 0, \tag{8}$$

with $\mathcal{H}_l = -24$ and $\mathcal{H}_{\mathrm{th}} = +24$ for the trefoil [Fig. 2(d)].

While we only visualized the E_x, E_z unlinking, each vector component pair undergoes separate transitions. Table II gives a better perspective for each vector component pair, showing results at $z = 0$ and $z = 5$. Since the trefoil topology is similar for E_x, E_y, B_x, B_y and the loop and thread topology is similar for E_z, B_z, there are several degenerate values for twist, linkage, and thread count. The closed-loop part $\mathcal{C}^l$ is nonzero only when a longitudinal component is involved ($\mathcal{C}^l = -2$ for pairs involving longitudinal polarizations), precisely canceled by the threading $\mathcal{T}$ of the open E_z and B_z null lines. Each mutual entry corresponds to a different observable's Stokes twist

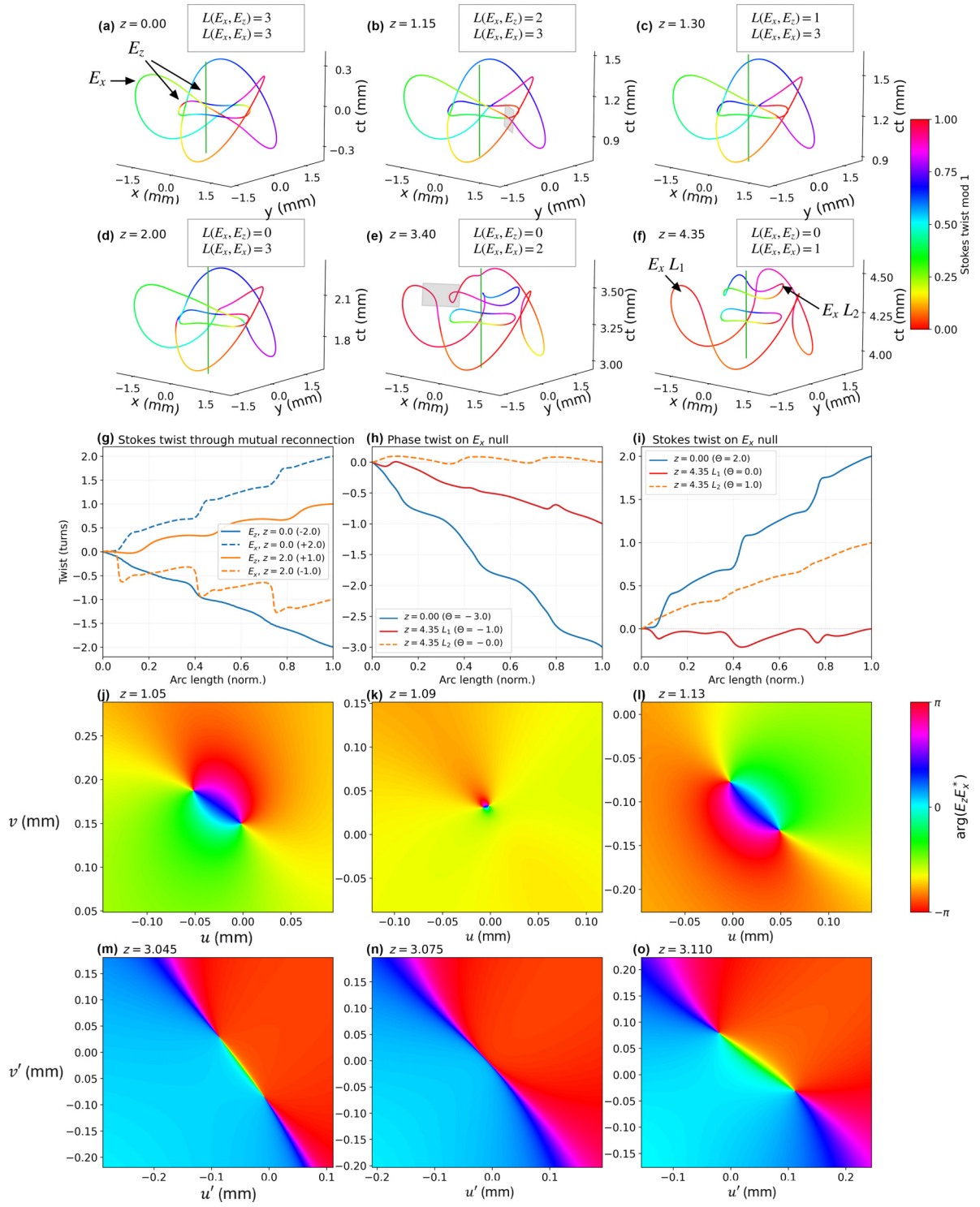


FIG. 1. Null-line topology through mutual and self-reconnection. (a)–(c) E_x and E_z null lines unlinking with propagation; the open E_z null line threads through all closed loops. Curves colored by cumulative Stokes twist. (d)–(f) The E_x trefoil unknots via self-reconnection with further propagation. (g) Electric spin Stokes twist $\arg(E_z^* E_x)$ along E_x and E_z null lines before and after mutual reconnection. (h) Self-phase twist along the E_x null line before and after self-reconnection. (i) Electric spin Stokes twist along E_x null line, same z values as (h). (j)–(l) Phase of $\arg(E_z^* E_x)$ on cross sections through the E_x-E_z crossing [gray square region in panel (b)]. (m)–(o) Phase of $\arg(E_z^* E_x)$ cross sections through the E_x self-reconnection [gray square region in panel (e)]. The null-line evolution is shown in SM Video 1 [28].

(Table I). As the E_x-E_z linking drops from 3 to 0, the electric spin Stokes twist compensates exactly. The same holds independently for the linear momentum (E_x, B_z), electromagnetic helicity (E_z, B_z) and (E_x, B_x), and magnetic spin (B_x, B_z). The longitudinal helicity (E_z, B_z) has nonzero threading due to the open lines of the longitudinal components, while the transverse helicity has zero threading from the purely closed loop trefoil curves.

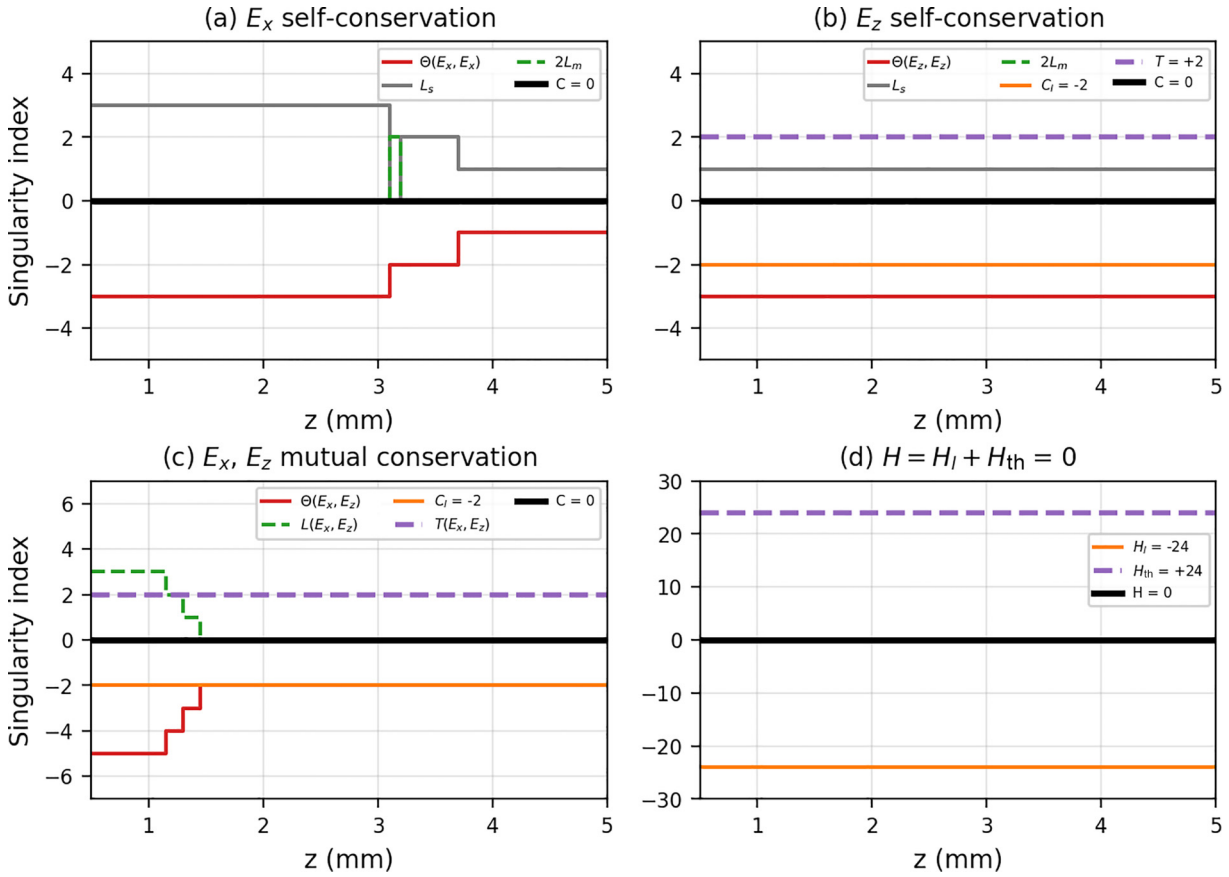


FIG. 2. $\mathcal{C} = 0$ verified through propagation. (a) E_x self-conservation: $\mathcal{C} = \Theta(E_x, E_x) + L_s + 2L_m = 0$ (black). (b) E_z self-conservation: the closed-loop part $\mathcal{C}_l = -2$ (orange) is offset by threading $\mathcal{T} = +2$ (purple dashed), giving $\mathcal{C} = 0$ (black). (c) E_x-E_z mutual conservation: $\mathcal{C}_l = \Theta(E_z|E_x) + L = -2$ (orange); $\mathcal{T} = +2$ (purple dashed); $\mathcal{C} = 0$ (black). (d) Total: $\mathcal{H}_l = -24$ (orange), $\mathcal{H}_{\text{th}} = +24$ (purple dashed), $\mathcal{H} = 0$ (black).

We also investigated additional knot types by varying the polynomial degrees (m, n) (Table III). The results show that the closed-loop contribution is $\mathcal{H}_l = -12m$, which depends only on m and is independent of the knot type n. The unknot, Hopf link, trefoil, and unlink, which are topologically distinct, all give $\mathcal{H}_l = -24$ when $m = 2$. In every case, the threading $\mathcal{H}_{\text{th}} = +12m$ cancels exactly, giving $\mathcal{H} = 0$.

The scaling $\mathcal{H}_l = -12m$ follows because m controls the number of open null lines created by the factor p^m, so the total threading scales with m but is independent of the braiding pattern set by q^n. The threading is also insensitive to chirality: replacing $q = \mathrm{i}(x + \mathrm{i}y)$ with its conjugate $\bar{q} = -\mathrm{i}(x - \mathrm{i}y)$ produces the mirror-image trefoil, but the threading numbers and $\mathcal{H}$ are unchanged.

TABLE II. Conservation matrix $\mathcal{C}$ for the trefoil beam at $z = 0$ and $z = 5$, showing redistribution of linkage and twist while each entry remains independently conserved.

			$z = 0$		$z = 5$				
Category	Component 1	Component 2	$\mathcal{C}$	$\Theta(b\|a)$	L	$\mathcal{T}$	$\Theta(b\|a)$	L	$\mathcal{T}$
Transverse, longitudinal	E_x, E_y, B_x, B_y	E_z, B_z	0	-5	$+3$	$+2$	-2	0	$+2$
Longitudinal, transverse	E_z, B_z	E_x, E_y, B_x, B_y	0	-3	$+3$	0	0	0	0
Category	Pair or component		$\mathcal{C}$	$\Theta(b\|a)$	L	$\mathcal{T}$	$\Theta(b\|a)$	L	$\mathcal{T}$
Transverse self	E_x, E_x, $E_y, E_y, B_x, B_x, B_y, B_y$		0	-3	$+3$	0	-1	$+1$	0
Longitudinal self	E_z, E_z, B_z, B_z		0	-3	$+1$	$+2$	-3	$+1$	$+2$
Longitudinal helicity	(E_z, B_z)		0	0	-2	$+2$	0	-2	$+2$
Transverse spin or helicity	(E_x, E_y), (E_x, B_x), (E_y, B_y)		0	-4	$+4$	0	-2	$+2$	0
Transverse magnetic spin	(B_x, B_y)		0	-5	$+5$	0	-2	$+2$	0
Longitudinal Poynting	(E_x, B_y), (E_y, B_x)		0	-7	$+7$	0	-7	$+7$	0

TABLE III. Threading for Milnor polynomials $p^m + q^n$. $\mathcal{H}_l$ is the closed-loop contribution (linking + twist), $\mathcal{H}_{\text{th}}$ is the open-line threading, and $\mathcal{H} = \mathcal{H}_l + \mathcal{H}_{\text{th}} = 0$ in every case.

Polynomial	(m, n)	Topology	$\mathcal{H}_l$	$\mathcal{H}_{\text{th}}$	$\mathcal{H}$
$p + q$	(1, 1)	Unknot	−12	+12	0
$p^2 + q$	(2, 1)	Unlink	−24	+24	0
$p^2 + q^2$	(2, 2)	Hopf link	−24	+24	0
$p^2 + q^3$	(2, 3)	Trefoil knot	−24	+24	0
$p^3 + q^3$	(3, 3)	Three-component link	−36	+36	0

IV. DISCUSSION

For a single scalar field, Berry and Dennis showed that the phase twist of a dislocation loop equals the threading strength [7], and Dennis connected this to the Călugăreanu decomposition [13,14]. Our conservation matrix extends this from a single framed curve to six families of curves framed by one another's phases, and from a static identity to a dynamical conservation law through reconnections. A key distinction is that reconnections can only occur in free-space propagation in polychromatic wave packets, not in monochromatic fields.

Fluid helicity degrades through viscous dissipation and magnetic helicity through resistive diffusion. In contrast, the invariants here hold at every propagation distance because they rest on the integer-valued argument principle rather than on an energy inequality. Although we numerically validate the matrix formulation here only for electromagnetic fields, it may apply to other systems with multiple complex scalar fields whose null lines form closed curves.

Spatiotemporal vortex reconnections have been demonstrated experimentally [15]. The conservation law predicts that any such closed-loop reconnection event must be accompanied by an exactly compensating twist in the electromagnetic observables, a testable signature accessible through measurement of the field components.

V. CONCLUSION

This work showed that spatiotemporal vortex knots undergo topology-changing reconnections with free-space propagation. When null lines of different vector components unlink, the electric spin, magnetic spin, linear momentum, and electromagnetic helicity densities, each built from a specific pair of field components, twist to exactly compensate the change in linking number. This compensation is enforced by the argument principle: the total for each component pair, combining mutual phase twist, geometric linking, and open-line threading, vanishes identically and remains exactly zero through all reconnection events. We believe these results will be beneficial for future applications that use spatiotemporal vortex knots and may improve understanding of fluid reconnection processes.

ACKNOWLEDGMENT

This work was supported by the Air Force Office of Scientific Research (AFOSR) under Award No. FA9550-25-1-0110.

DATA AVAILABILITY

The numerical data and analysis code that support the findings of this study are available from the corresponding author upon reasonable request.

[1] M. W. Scheeler, D. Kleckner, D. Proment, G. L. Kindlmann, and W. T. M. Irvine, Helicity conservation by flow across scales in reconnecting vortex links and knots, Proc. Natl. Acad. Sci. USA **111**, 15350 (2014).

[2] D. Kleckner and W. T. M. Irvine, Creation and dynamics of knotted vortices, Nat. Phys. **9**, 253 (2013).

[3] H. K. Moffatt and R. L. Ricca, Helicity and the Călugăreanu invariant, Proc. R. Soc. Lond. A **439**, 411 (1992).

[4] G. Călugăreanu, Sur les classes d'isotopie des noeuds tridimensionnels et leurs invariants, Czechoslovak Math. J. **11**, 588 (1961).

[5] J. B. Taylor, Relaxation of toroidal plasma and generation of reverse magnetic fields, Phys. Rev. Lett. **33**, 1139 (1974).

[6] M. A. Berger, Introduction to magnetic helicity, Plasma Phys. Control. Fusion **41**, B167 (1999).

[7] M. V. Berry and M. R. Dennis, Knotted and linked phase singularities in monochromatic waves, Proc. R. Soc. Lond. A **457**, 2251 (2001).

[8] M. R. Dennis, R. P. King, B. Jack, K. O'Holleran, and M. J. Padgett, Isolated optical vortex knots, Nat. Phys. **6**, 118 (2010).

[9] H. Larocque, A. D'Errico, M. F. Ferrer-Garcia, A. Carmi, E. Cohen, and E. Karimi, Optical framed knots as information carriers, Nat. Commun. **11**, 5119 (2020).

[10] B. Bode, Stable knots and links in electromagnetic fields, Commun. Math. Phys. **387**, 1757 (2021).

[11] D. Sugic, R. Droop, E. Otte, D. Ehrmanntraut, F. Nori, J. Ruostekoski, C. Denz, and M. R. Dennis, Particle-like topologies in light, Nat. Commun. **12**, 6785 (2021).

[12] Y. Shen, Q. Zhang, P. Shi, L. Du, X. Yuan, and A. V. Zayats, Optical skyrmions and other topological quasiparticles of light, Nat. Photon. **18**, 15 (2024).

[13] M. R. Dennis, Topological singularities in wave fields. Ph.D. thesis, University of Bristol, 2001.

[14] M. R. Dennis, Local phase structure of wave dislocation lines: Twist and twirl, J. Opt. A Pure Appl. Opt. **6**, S202 (2004).

[15] J. M. Adams, I. Agha, and A. Chong, Spatiotemporal optical vortex reconnections of multi-vortices, Sci. Rep. **14**, 5483 (2024).

[16] J. M. Adams and A. Chong, Spatiotemporal optical vortex reconnections of loop vortices, Nanophotonics **14**, 729 (2025).

[17] T. Bucher, A. Gorlach, A. Niedermayr, Q. Yan, H. Nahari, K. Wang, R. Ruimy, Y. Adiv, M. Yannai, T. L. Abudi, E. Janzen, C. Spaegele, C. Roques-Carmes, J. H. Edgar, F. H. L. Koppens, G. M. Vanacore, H. H. Sheinfux, S. Tsesses, and I. Kaminer, Superluminal correlations in ensembles of optical phase singularities, Nature (London) **651**, 920 (2026).

[18] J. M. Adams, Spatiotemporal optical vortex phenomena, Ph.D. thesis, University of Dayton, 2024.

[19] Y. Zhou, N. Zhang, A. Zhou, Z. Zhang, J. Liu, C. Liang, S. A. Ponomarenko, Q. Zhan, Y. Cai, and X. Liu, Spatiotemporally localized optical links and knots, Nat. Commun. **17**, 6027 (2026).

[20] W. Wang, B. Jüttler, D. Zheng, and Y. Liu, Computation of rotation minimizing frames, ACM Trans. Graph. **27**, 2 (2008).

[21] L. V. Ahlfors, *Complex Analysis: An Introduction to the Theory of Analytic Functions of One Complex Variable*, 3rd ed. (McGraw-Hill, New York, 1979).

[22] K. Domina, P. Alonso-González, A. Bylinkin, M. Barra-Burillo, A. I. F. Tresguerres-Mata, F. J. Alfaro-Mozaz, S. Vélez, F. Casanova, L. E. Hueso, R. Hillenbrand, K. Y. Bliokh, and A. Y. Nikitin, High-intensity wave vortices around subwavelength holes: From ocean tides to nanooptics, Newton **1**, 100060 (2025).

[23] V. Guillemin and A. Pollack, *Differential Topology* (Prentice-Hall, Englewood Cliffs, NJ, 1974).

[24] R. L. Ricca and B. Nipoti, Gauss' linking number revisited, J. Knot Theory Ramif. **20**, 1325 (2011).

[25] N. Mata-Cervera, Z. Guo, and Y. Shen, Unfolding unstable skyrmionic polarization textures, Laser Photon. Rev. e71667 (2026).

[26] N. Mata-Cervera, D. K. Sharma, Y. Shen, R. Paniagua-Dominguez, and M. A. Porras, Skyrmionic polarization texture around the phase singularity of optical vortices, Phys. Rev. Lett. **135**, 033805 (2025).

[27] J. Milnor, *Singular Points of Complex Hypersurfaces* (Princeton University Press, Princeton, 1968).

[28] See Supplemental Material at http://link.aps.org/supplemental/10.1103/ny6g-sm2k for the skyrmion-number calculation, polarization textures and convergence checks, and a video of the vortex-line dynamics, which includes Refs. [29–32].

[29] Y. Shen, H. Wang, and S. Fan, Free-space topological optical textures: Tutorial, Adv. Opt. Photon. **17**, 295 (2025).

[30] B. Berg and M. Lüscher, Definition and statistical distributions of a topological number in the lattice O(3) σ-model, Nucl. Phys. B. **190**, 412 (1981).

[31] A. A. Wang, Z. Zhao, Y. Ma, Y. Cai, R. Zhang, X. Shang, Y. Zhang, J. Qin, Z.-K. Pong, T. Marozsák, B. Chen, H. He, L. Luo, M. J. Booth, S. J. Elston, S. M. Morris, and C. He, Topological protection of optical skyrmions through complex media, Light Sci. Appl. **13**, 314 (2024).

[32] X. S. Wang, H. Y. Yuan, and X. R. Wang, A theory on skyrmion size, Commun. Phys. **1**, 31 (2018).